Electronic Supplementary Material (ESI) for Journal of Materials Chemistry A.

Supporting Information

Transition Metal-Substituted Lead Halide Perovskite Absorbers

M. D. Sampson, J.-S. Park, R. D. Schaller, M. K. Y. Chan,* and A. B. F. Martinson*

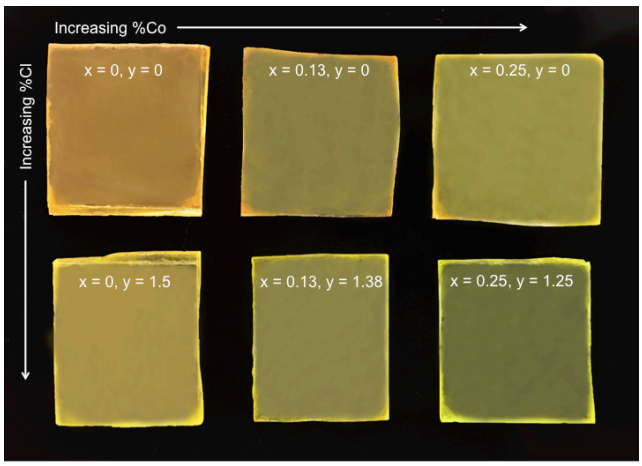

Figure S1. Photograph of $MAPb_{1-x}Co_xBr_{3-y}Cl_y$ thin films on FQ.

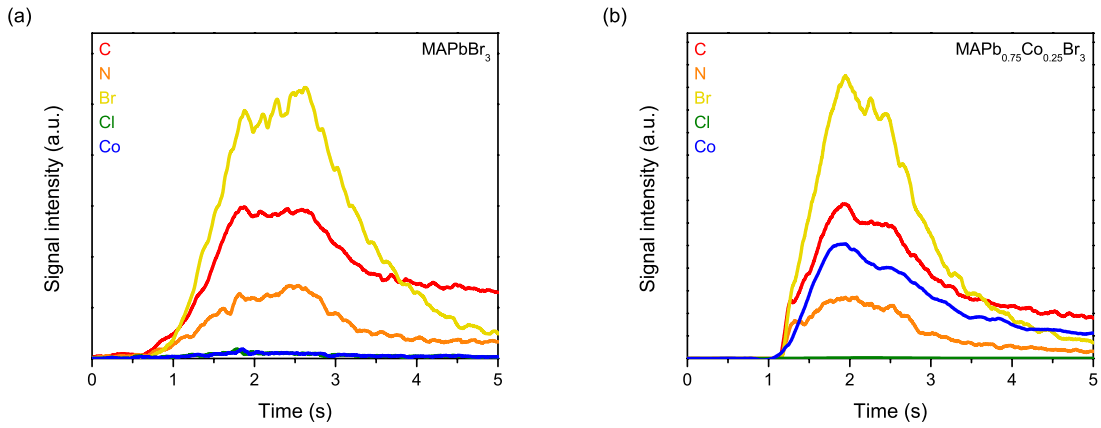

Figure S2. Glow discharge optical emission spectroscopy (GDOES) of (a) $MAPbBr_3$ and (b) $MAPb_{0.75}Co_{0.25}Br_3$ thin films. The signals for oxygen and hydrogen have been omitted for clarity.

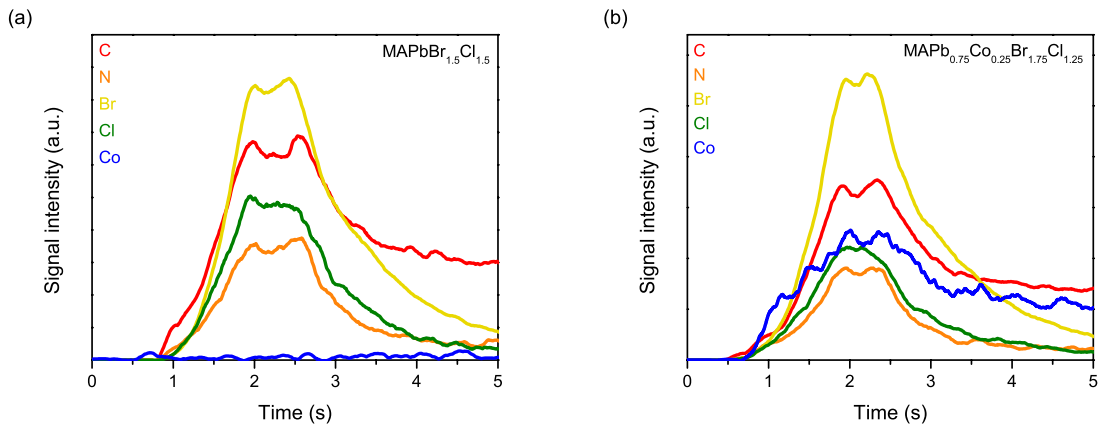

Figure S3. Glow discharge optical emission spectroscopy (GDOES) of (a) $MAPbBr_{1.5}Cl_{1.5}$ and (b) $MAPb_{0.75}Co_{0.25}Br_{1.75}Cl_{1.25}$ thin films. The signals for oxygen and hydrogen have been omitted for clarity.

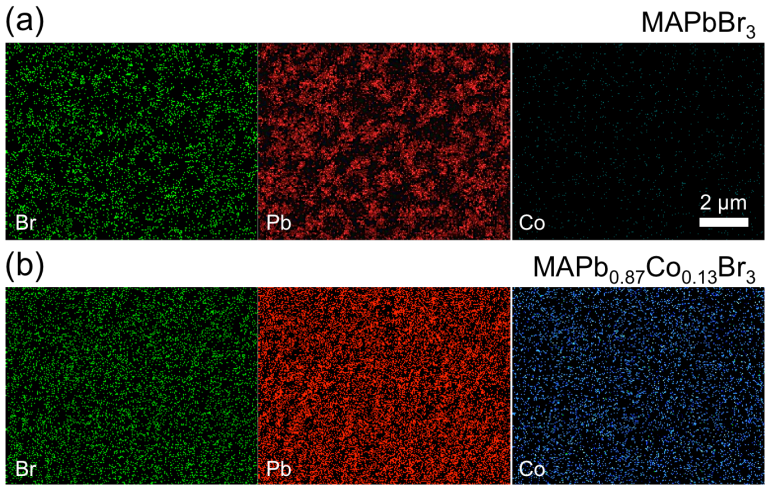

Figure S4. EDX elemental mapping of (a) $MAPbBr_3$ and (b) $MAPb_{0.87}Co_{0.13}Br_3$ thin films under the same data acquisition parameters. Green = Br, red = Pb, and blue = Co.

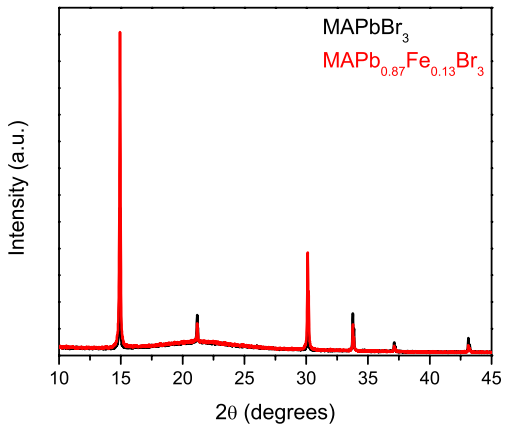

Figure S5. XRD patterns of $MAPbBr_3$ (black) and Fe-substituted $MAPb_{0.87}Fe_{0.25}Br_3$ (red) thin films.

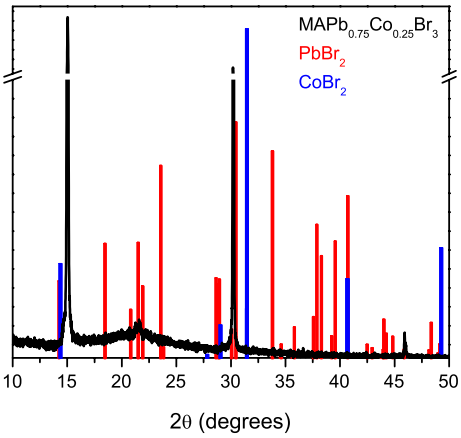

Figure S6. Predicted XRD patterns for $PbBr_2$ (red) and $CoBr_2$ (blue), with the XRD pattern for a $MAPb_{0.75}Co_{0.25}Br_3$ (black) thin film shown for comparison.

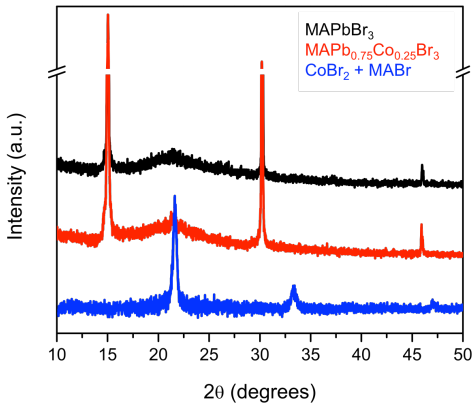

Figure S7. XRD pattern of a control film consisting of a 1:1 ratio of $CoBr_2$ to MABr (blue), with XRD patterns for $MAPbBr_3$ (black) and $MAPb_{0.75}Co_{0.25}Br_3$ (red) thin films shown for comparison.

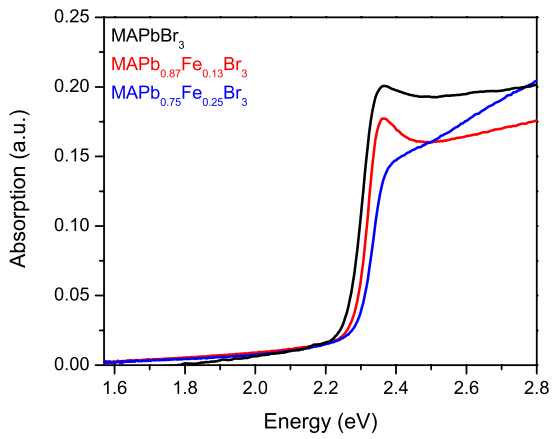

Figure S8. Absorption spectra of $MAPbBr_3$ (black), $MAPb_{0.87}Fe_{0.13}Br_3$ (red), and $MAPb_{0.75}Fe_{0.25}Br_3$ (blue) thin films, showing no mid-band gap absorption.

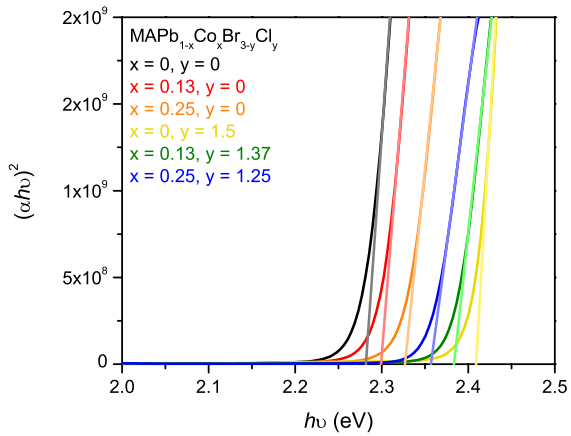

Figure S9. Tauc plots of the band gap for $MAPb_{1-x}Co_xBr_{3-y}Cl_y$ thin films on FQ.

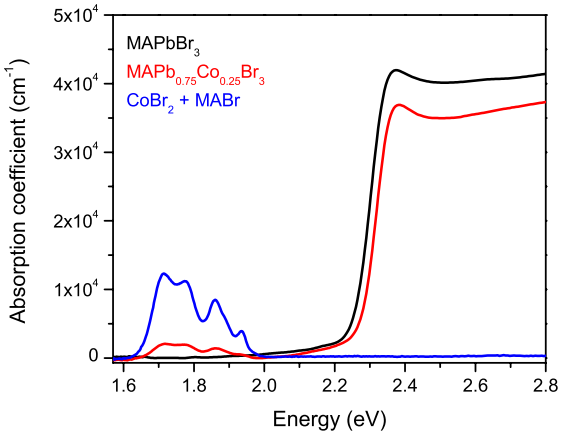

Figure S10. Absorption spectrum of a control film consisting of a 1:1 ratio of $CoBr_2$ to MABr (blue), with the absorption spectra for $MAPbBr_3$ (black) and $MAPb_{0.75}Co_{0.25}Br_3$ (red) thin films shown for comparison.

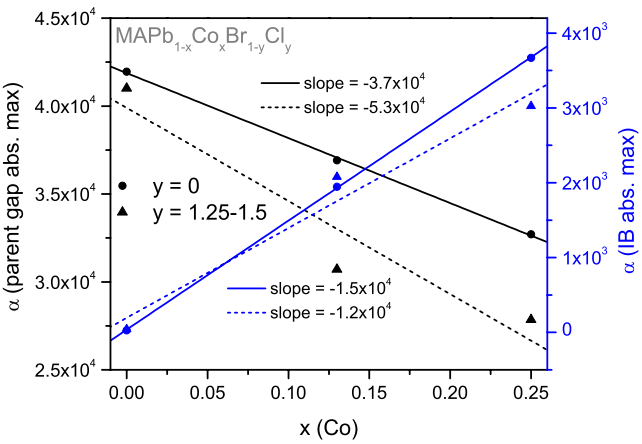

Figure S11. Peak absorption coefficient (α) for the parent gap (left axis) and Co-based mid-gap states (right axis) as a function of the amount of Co in the substituted film (x) for $MAPb_{1-x}Co_xBr_{1-y}Cl_y$. Linear fits of the data are shown to indicate trends.

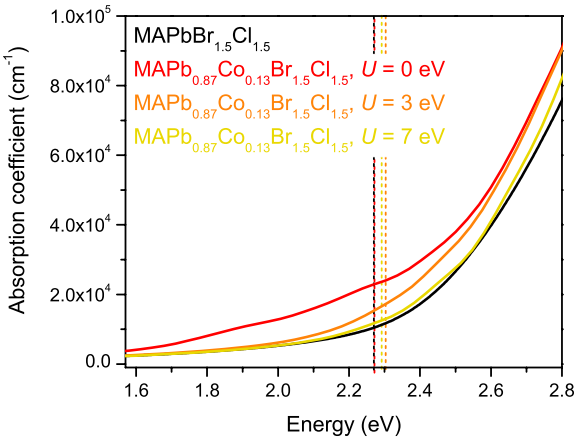

Figure S12. Calculated absorption coefficient of $MAPb_{0.87}Co_{0.13}Br_{1.5}Cl_{1.5}$ with U values (for Co 3*d* orbitals) of 0 (red), 3 (orange), and 7 eV (yellow) as compared to the calculated absorption coefficient of $MAPbBr_{1.5}Cl_{1.5}$ (black). The calculated band gaps are indicated with vertical dotted lines.

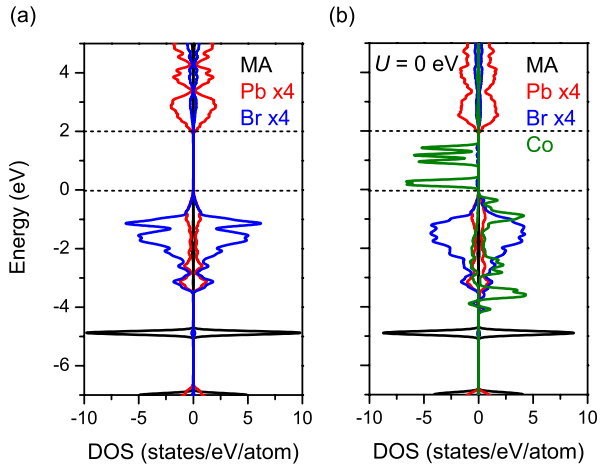

Figure S13. Calculated electronic structure of (a) $MAPbBr_3$ and (b) $MAPb_{0.87}Co_{0.13}Br_3$ with a Hubbard U = 0 eV used for Co *d* orbitals. The dashed horizontal lines represent the band edges of pure $MAPbBr_3$ estimated by N core level as reference in the calculations.

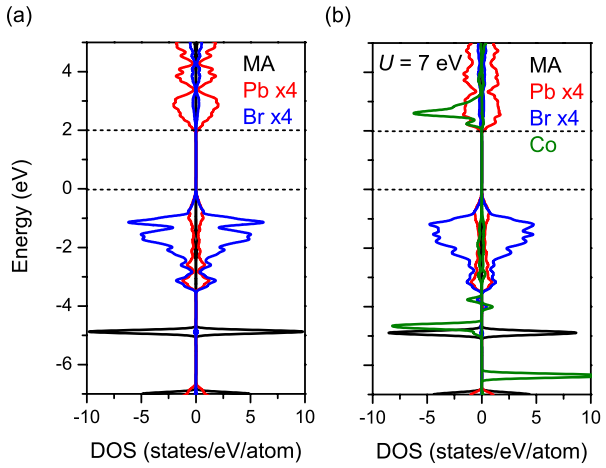

Figure S14. Calculated electronic structure of (a) $MAPbBr_3$ and (b) $MAPb_{0.87}Co_{0.13}Br_3$ with a Hubbard U = 7 eV used for Co d orbitals. The dashed horizontal lines represent the band edges of pure $MAPbBr_3$ estimated by N core level as reference in the calculations.

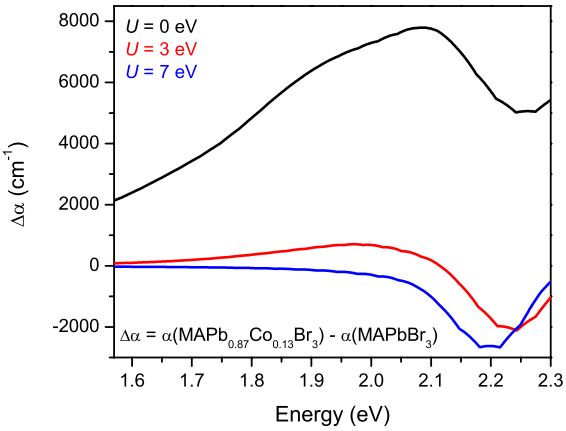

Figure S15. Change in absorption coefficient (Δα) of $MAPb_{0.87}Co_{0.13}Br_3$ from $MAPbBr_3$ for U values (for Co 3d orbitals) of 0 (black), 3 (red), and 7 eV (blue).

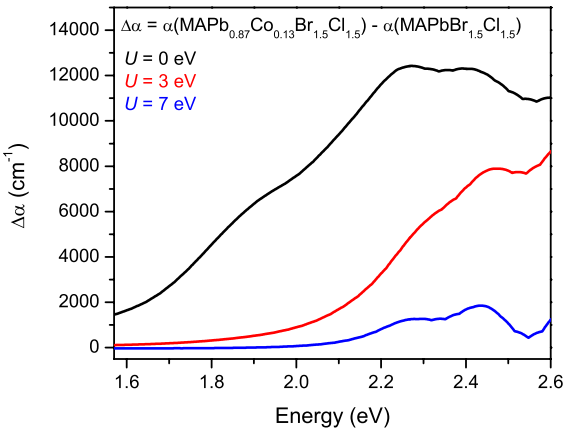

Figure S16. Change in absorption coefficient (Δα) of $MAPb_{0.87}Co_{0.13}Br_{1.5}Cl_{1.5}$ from $MAPbBr_{1.5}Cl_{1.5}$ for U values (for Co 3d orbitals) of 0 (black), 3 (red), and 7 eV (blue).

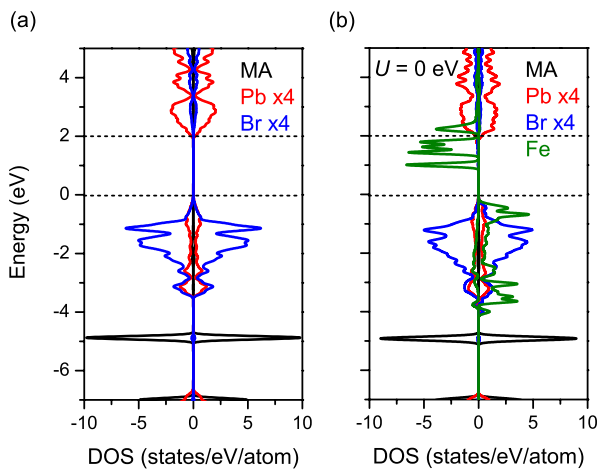

Figure S17. Calculated electronic structure of (a) $MAPbBr_3$ and (b) $MAPb_{0.87}Fe_{0.13}Br_3$ with a Hubbard U = 0 eV used for Fe *d* orbitals. The dashed horizontal lines represent the band edges of pure $MAPbBr_3$ estimated by N core level as reference in the calculations.

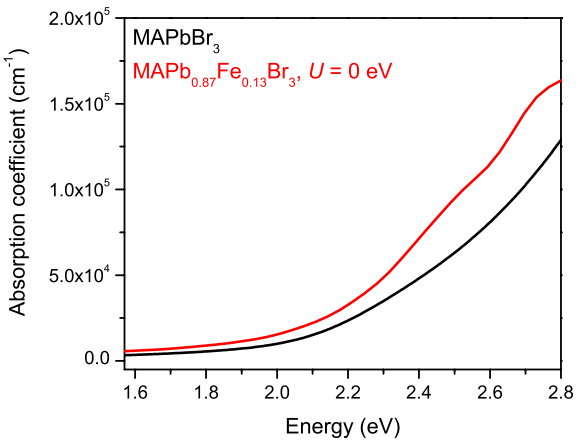

Figure S18. Calculated absorption coefficient of $MAPb_{0.87}Fe_{0.13}Br_3$ with a Hubbard U = 0 eV used for Fe *d* orbitals (red) as compared to the calculated absorption coefficient of $MAPbBr_3$ (black).

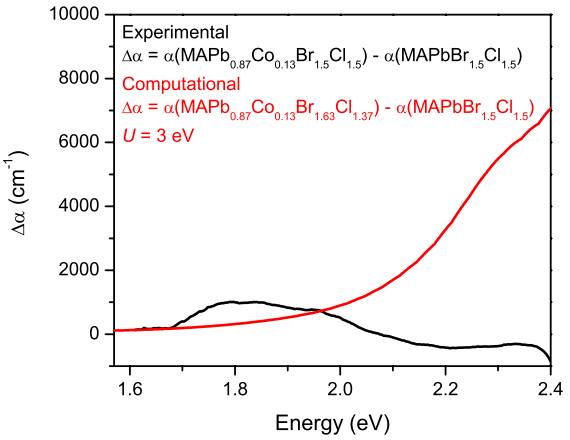

Figure S19. Change in absorption coefficient (Δα) of $MAPb_{0.87}Co_{0.13}Br_{1.5}Cl_{1.5}$ from $MAPbBr_{1.5}Cl_{1.5}$ for experimental (black) and computations (red, U = 3 eV). The experimental difference plot has a Br and Cl content of $Br_{1.63}Cl_{1.37}$.

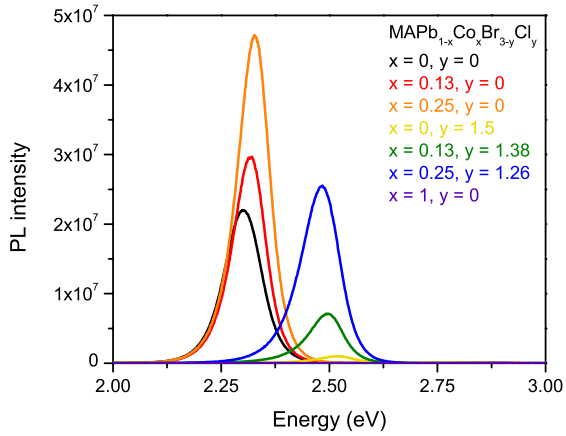

Figure S20. Non-normalized steady state PL spectra of of $MAPb_{1-x}Co_xBr_{3-y}Cl_y$ thin films. The spectrum of a control film consisting of a 1:1 ratio of $CoBr_2$ to MABr is shown in purple.

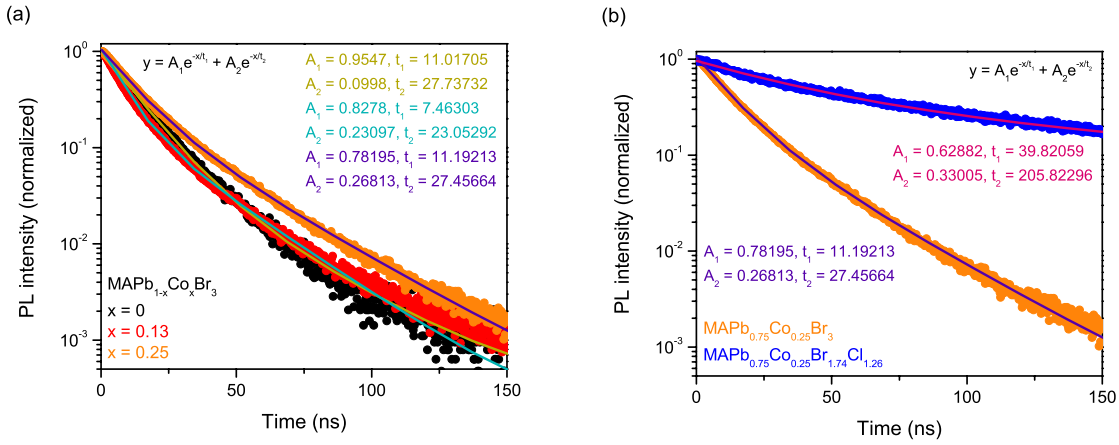

Figure S21. Exponential fits for the time-resolved PL data shown in Figure 4.

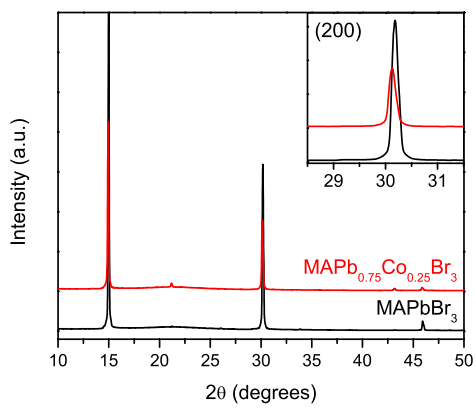

Figure S22. XRD pattern for $MAPbBr_3$ (black) and $MAPb_{0.75}Co_{0.25}Br_3$ (red) thin films taken with a diffractometer containing a monochromator to filter out Cu *Kβ* irradiation. Inset shows zoomed (200) peaks.

Table S1. Band gaps extracted from Tauc plots and PL peaks.

$MAPb_{1-x}Co_xBr_{1-y}Cl_y$	Band Gap (eV)	PL peak (eV)
x = 0, y = 0	2.27	2.30
x = 0.13, y = 0	2.29	2.32
x = 0.25, y = 0	2.31	2.33
x = 0, y = 1.5	2.40	2.52
x = 0.13, y = 1.37	2.37	2.50
x = 0.25, y = 1.25	2.35	2.48

Table S2. Lifetimes extracted from exponential fits of time-resolved PL data.

$MAPb_{1-x}Co_xBr_{1-y}Cl_y$	τ_1 (ns)	τ_2 (ns)
x = 0, y = 0	11.0	27.7
x = 0.13, y = 0	7.46	23.1
x = 0.25, y = 0	11.2	27.5
x = 0.25, y = 1.25	39.8	206